J Membrane Biol (2016) 249:31–39
DOI 10.1007/s00232-015-9843-4

Cell Electrofusion in Centrifuged Erythrocyte Pellets Assessed by Dielectric Spectroscopy

Koji Asami[1]

Received: 15 January 2015 / Accepted: 18 September 2015 / Published online: 25 September 2015

Abstract We have characterized cell electrofusion in cell pellets by dielectric spectroscopy. Cell pellets were formed from horse erythrocyte suspensions by centrifugation and were subjected to intense AC pulses. The dielectric spectra of the pellets were measured over a frequency range of 10 Hz to 10 MHz. The application of AC pulses caused low-frequency (LF) dielectric relaxation below about 100 kHz. The LF dielectric relaxation was markedly affected not only by pretreatment of cells at 50 °C, which disrupts the spectrin network of erythrocytes, but also by the parameters of the AC pulses (frequency of the sine wave and repeat count of the pulses). The occurrence of the LF dielectric relaxation was qualitatively accounted for by modeling fusion products in the pellet by prolate spheroidal cells whose long axes run parallel to the applied electric field.

Keywords Dielectric spectroscopy · Cell electrofusion · Erythrocytes · Centrifuged cell pellets · Spectrin network · Spheroidal shell model

Introduction

Cell electrofusion is an important technique to prepare either hybridoma cells that produce monoclonal antibodies or giant cells accessible to the patch clamp technique for electrophysiological studies (Zimmermann 1982; Terpitz et al. 2012). The electrofusion requires two processes: contacting cells and application of intense electric pulses. In order to make close contact between cells, various methods have been adopted. The most widely used method is pearl chain formation by dielectrophoresis. The adherence method uses cell contact established spontaneously in confluent culture (Finaz et al. 1984; Salomskaite-Davalgiene et al. 2009), in tumor tissues (Mekid and Mir 2000; Salomskaite-Davalgiene et al. 2009), and by plating cells at suitable concentration (Usaj et al. 2010). Another method is to use mechanically forced cell-to-cell contacts that are achieved in centrifuged cell pellets (Takahashi et al. 1991; Abidor et al. 1993, 1994; Li et al. 1996) and in cell pellets trapped on membrane filters (Jaroszeski et al. 1994).

The morphology of fusion products induced by electric pulses can be directly observed under an optical microscope if cells spread on transparent substrates. In the case of thick cell aggregates like cell pellets and tissues, however, in situ microscopic examination becomes difficult. Usually, morphological analysis is carried out either by taking cells out of the pellets, which procedure is liable to damage cells or by time-consuming thin-sectioning of fixed tissues. Non-invasive and in situ techniques, therefore, are required to assess fusion products in cell pellets and tissues. Abidor et al. (1993, 1994) applied electric impedance measurement to centrifuged cell pellets and discussed the fusion process from the resistance and capacitance of the cell pellets determined using a 10 kHz AC signal or a rectangular pulse. The studies, however, provided little information on the morphology of fusion products. In this paper, dielectric spectroscopy has been proposed to characterize the morphology of fusion products in centrifuged cell pellets.

Biological cells and tissues show dielectric dispersion due to interfacial polarization that is sensitive to cell shape, cell-to-cell interactions and cell aggregation. Hence, dielectric

✉ Koji Asami
asami@e.kuicr.kyoto-u.ac.jp

[1] Institute for Chemical Research, Kyoto University, Uji, Kyoto 611-0011, Japan

spectroscopy has been applied to monitoring of morphological changes in various biological phenomena: cell division (Asami et al. 1999), cell aggregation (Irimajiri et al. 1996; Jaroszynski et al. 2002), blood coagulation (Hayashi et al. 2010), tissue formation (Daoud et al. 2012), and hemolysis (Asami 2012). The experimental results have been successfully simulated by taking into account the morphological changes (Sekine et al. 2005; Asami 2007; Asami and Sekine 2007a, b; Asami 2012). The previous studies suggest that dielectric spectroscopy would be feasible for solving the problems concerned in this study.

Materials and Methods

Preparation of Erythrocytes

Erythrocytes were obtained from preserved horse blood purchased from Nippon Biotest Lab. (Tokyo, Japan). The blood specimens were centrifuged at $300\times g$ for 10 min to remove the plasma and buffy coat, and the collected erythrocytes were washed twice with an isotonic solution containing 150 mM NaCl and 5 mM Na-phosphate (Na-P) buffer (pH 7.2).

Electrofusion in Erythrocyte Pellets

An electrofusion chamber capable of centrifugation, which was similar to that reported by Takahashi et al. (1991), consisted of two parts made of Lucite: a cylindrical cup with a disk Pt electrode at the bottom and a cylindrical plug with a disk Pt electrode at the end (Fig. 1). The Pt electrodes of about 5 mm in diameter were platinized to reduce the electrode polarization (EP) effect. The cup was filled with an erythrocyte suspension and the plug was fixed as shown in Fig. 1a, the electrode distance being about 5 mm. The chamber was centrifuged at $500\times g$ for 10 min by a swing type centrifuge to form an erythrocyte pellet of a uniform thickness on the bottom electrode. The pellet was about 1 mm thick when the suspension contained erythrocytes at a volume fraction of about 0.1.

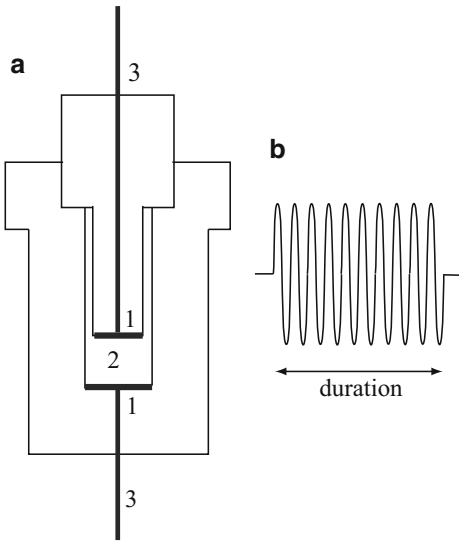

Fig. 1 **a** A chamber capable of centrifugation, used for both electrofusion and dielectric measurement. (*1*) electrodes, (*2*) a sample cavity, (*3*) lead wires to connect with an AC pulse generator or with an impedance analyzer. **b** The waveform of the AC pulse used for electrofusion

The pellet was subjected to intense alternating field pulses (AC pulses) through the electrodes of the chamber. One AC pulse had a duration of 10 ms and, unless otherwise noted, the frequency of the sine wave was 1 kHz, i.e., there were 10 cycles in the duration (Fig. 1b). The peak-to-peak voltage was 360 V. Several AC pulses were applied at an interval of about 1 s. The AC pulses were generated with a 1946 Multifunction Synthesizer (NF Corporation, Japan) and were amplified with an HAS4051 High Speed Bipolar Amplifier (NF Corporation, Japan).

Dielectric Measurement

The admittance of the fusion chamber filled with a sample was measured with a 4192A Impedance Analyzer (Hewlett-Packard). The measured capacitance and conductance was converted to the relative permittivity and conductivity of the sample using the cell constant of 0.039 pF and the stray capacitance of 0.30 pF of the chamber, which were determined from the capacitance values measured for the chamber filled with distilled water and the empty chamber.

Results

Intact Erythrocytes

A suspension of erythrocytes was centrifuged to form a cell pellet on the bottom electrode in the fusion chamber. Ten AC pulses were applied to the chamber at an interval of about 1 s. Dielectric spectra (frequency dependence of relative permittivity ε and conductivity κ) were measured in the following order: the initial cell suspension, after centrifugation, after pulse application, and finally when the pulsed pellet and the supernatant were mixed uniformly and centrifuged again (Fig. 2). The cell suspension showed dielectric relaxation around a few MHz together with the EP effect including a large increase in ε below 100 kHz and a decrease in κ below 1 kHz. After the formation of the pellet by centrifugation, dielectric relaxation became about 10 times larger in intensity than that of the cell suspension, and the EP effect shifted toward lower frequencies because

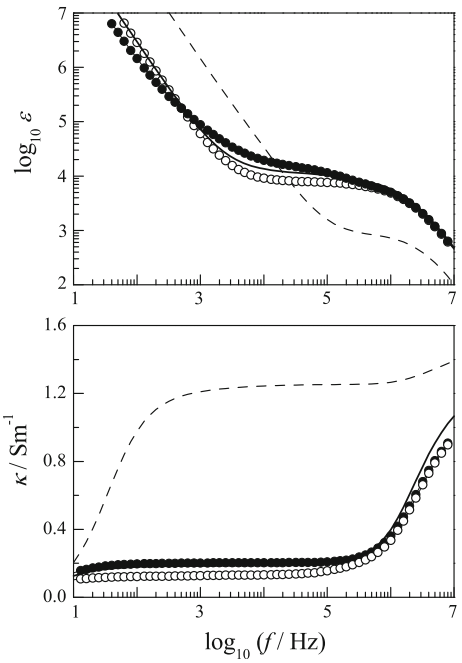

Fig. 2 Frequency (f) dependence of the relative permittivity (ε) and conductivity (κ) measured sequentially for an erythrocyte suspension (*dashed line*), after centrifugation (*open circle*), after pulse application (*closed circle*), and when cells in the pulsed pellet were re-suspended and centrifuged (*solid line*)

of a decrease in κ. The pulse application caused dielectric relaxation at low frequencies [hereafter, low-frequency (LF) relaxation] in addition to the dielectric relaxation around 1 MHz [high-frequency (HF) relaxation]. The occurrence of the LF relaxation accompanied a reduction in κ below 100 kHz, which may correspond to the increase of the pellet resistance reported by Abidor et al. (1994). When cells in the pulsed pellet were re-suspended and centrifuged, the LF relaxation was reduced in intensity while the HF relaxation was mostly unchanged.

Effects of Heat Treatment

It is known that disruption of the spectrin network by heat treatment affects the morphology of fusion products. Linear chains of fused erythrocytes induced by the pulse application were quickly converted into giant spherical cells when erythrocytes were pre-incubated in 220 mM sucrose and 20 mM Na-P (7.4) at 47 °C for 10 min (Chemomordik and Sowers 1991). Similar results were reported for erythrocytes treated at 50 °C (Glaser and Donath 1987). Since the deformation of fused cells was observed when electrofusion was performed with pearl-chains of cells formed in dilute cell suspensions, the question is raised whether the deformation occurs in closely packed cell pellets. Thus, effects of heat treatment on fusion products in the centrifuged cell pellets have been examined by dielectric spectroscopy. Erythrocytes were incubated in an isotonic solution containing 150 mM NaCl and 5 mM Na-P (7.2) at 50 °C for 10 min. Dielectric measurement was performed in the same procedure as that for intact cells, and the results are shown in Fig. 3. The dielectric spectra measured for the initial suspension and after centrifugation were little different from those of intact cells without heat treatment. Application of the same AC pulses as in Fig. 2 induced the LF relaxation whose intensity was much larger than that obtained for intact erythrocytes. When the cells in the pulsed pellet were re-suspended and centrifuged, the LF relaxation diminished completely but the HF relaxation changed slightly.

Analysis of Dielectric Spectra Using the Cole–Cole Equation

In order to determine the dielectric relaxation parameters of the LF and HF relaxation, the dielectric spectra were analyzed using an empirical equation (Asami 2012):

$$\varepsilon^* = \varepsilon_h + \frac{\Delta\varepsilon_H}{1+(\mathrm{j}f/f_{cH})^{\beta_H}} + \frac{\Delta\varepsilon_L}{1+(\mathrm{j}f/f_{cL})^{\beta_L}} + \frac{\kappa_l}{\mathrm{j}2\pi f\varepsilon_0} + Af^{-m}, \quad (1)$$

where j is the imaginary unit and ε_0 is the permittivity of vacuum. This equation contains two Cole–Cole relaxation

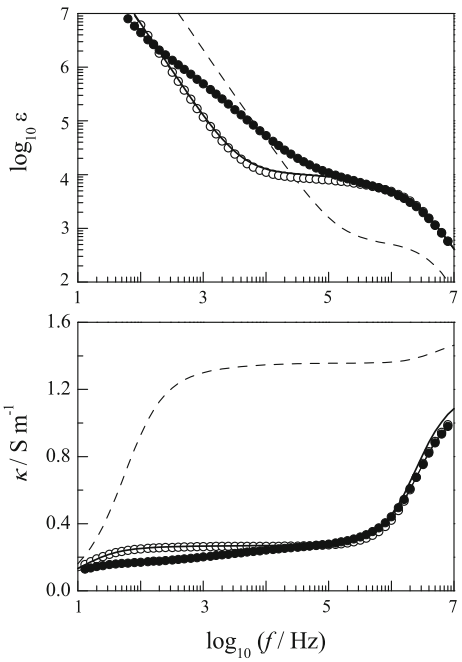

Fig. 3 Frequency (f) dependence of the relative permittivity (ε) and conductivity (κ) measured sequentially for a suspension of heat-treated erythrocytes (*dashed line*), after centrifugation (*open circle*), after pulse application (*closed circle*), and when the pulsed palette and the supernatant were mixed uniformly and centrifuged (*solid line*)

terms (subscripts H and L refer to the HF and the LF relaxations, respectively) and an EP term Af^{-m} with constants A and m. $\Delta\varepsilon$, f_c, and β are the intensity, the characteristic frequency, and the broadening factor of the Cole–Cole relaxation, respectively; ε_h is the high-frequency limit of relative permittivity and κ_l is the LF limit of conductivity. The values of ε_h, $\Delta\varepsilon_L$, f_{cL}, β_L, $\Delta\varepsilon_H$, f_{cH}, β_H, A, and m in Eq. (1) were determined from the real part of the dielectric spectra using the non-linear least squares method to minimize the residual χ^2

$$\chi^2 = \sum_i \left\{\log \mathrm{Re}\left[\varepsilon^*_{ob}(f_i)\right] - \log \mathrm{Re}\left[\varepsilon^*_{th}(f_i)\right]\right\}^2, \qquad (2)$$

where $\mathrm{Re}\left[\varepsilon^*_{ob}(f_i)\right]$ and $\mathrm{Re}\left[\varepsilon^*_{th}(f_i)\right]$ are the real parts of the observed and theoretical complex relative permittivities, respectively.

Figure 4 shows examples of the curve fitting with the dielectric spectra shown in Fig. 3. The dielectric spectra measured after centrifugation and after pulse application were well represented by the HF relaxation alone and by a sum of the HF and LF relaxations, respectively. The best-fit parameters for the LF and HF relaxations are listed in Table 1, which also contains the relaxation parameters for the dielectric spectrum obtained by suspending of cells in the pulsed pellet followed by centrifugation (procedure 3). The value of $\Delta\varepsilon_L$ was more than 100 times larger than that of $\Delta\varepsilon_H$. The pulse application (procedure 2) decreased the $\Delta\varepsilon_H$ and increased the f_{cH}, and the opposite changes were caused in the HF relaxation by procedure 3. The value of β_L was smaller than that of β_H, indicating the LF relaxation distributed over a wider frequency range than the HF relaxation. The values of m were consistent among the spectra, confirming reasonable correction for the EP effect.

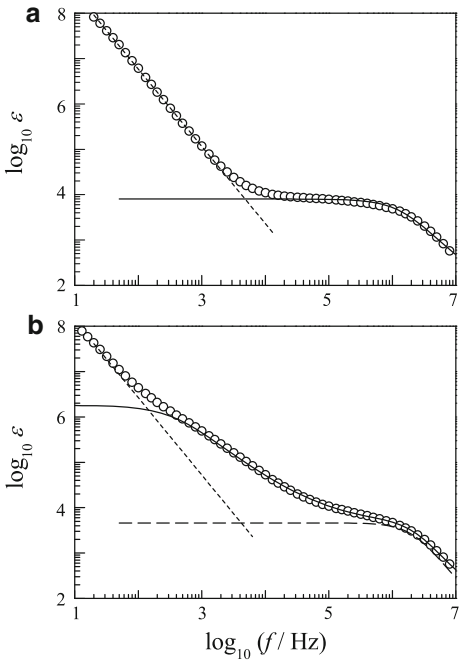

Fig. 4 Separation of the HF and LF relaxation and correction for the electrode polarization effect by curve fitting. Equation (1) was fitted to the dielectric spectra measured before **a** and after **b** pulse application (shown in Fig. 3). The solid curves calculated from the parameter values in Table 1 are separated from the electrode polarization effect (*dotted line*). The *dashed line* in **b** indicates the HF relaxation

Effects of Pulse Conditions

Since much larger changes in $\Delta\varepsilon_L$ were obtained with heat-treated erythrocytes than with intact ones, effects of AC pulse conditions were studied with heat-treated erythrocytes. AC pulses were repeatedly applied to the pellets at an interval of 1 s. Effects of the repeat count N_r of the pulses on the $\Delta\varepsilon_L$ and characteristic frequency f_{cL} of the LF relaxation were examined (Fig. 5). The $\Delta\varepsilon_L$ increased with N_r and tended to level off, which was accompanied with a decrease in f_{cL}. With increasing N_r, the $\Delta\varepsilon_H$ decreased slightly, whereas the f_{cH} was mostly unchanged.

Takahashi et al. (1991) reported that the yield of hybridoma produced by AC pulses depended on the frequency f_p of the sine wave in the AC pulses. Effects of the f_p on the $\Delta\varepsilon_L$ were examined in the case of $N_r = 10$, being shown in Fig. 6. The $\Delta\varepsilon_L$ rapidly decreased below 300 Hz and the efficient frequency was between 300 Hz and 1 kHz, which was slightly lower than that reported for hybridoma production.

Morphology of Fusion Products

After pulse application, cells were taken out of the pellets and were observed by optical microscopy. Figure 7 shows the phase contrast micrographs of the cells. The fusion products for intact erythrocytes without heat treatment were stable chains of cells, whereas those for heat-treated cells were giant spherical cells. The results are consistent with the previous report (Chemomordik and Sowers 1991) that, when spectrin networks of erythrocytes were disrupted, fusion products changed quickly from chains of cells to giant spherical cells. However, it is not clear whether the giant spherical cells existed in the pulsed pellet or were formed by re-suspending of cells in the pellet. This issue will be considered in "Discussion" section.

Discussion

The experimental results suggest that the LF relaxation is due to fusion products in the pellets. It is known that application of intense electric pulses induces chains of

Table 1 Dielectric relaxation parameters determined by fitting Eq. (1) to the spectra obtained after succeeding procedures: (1) centrifugation, (2) pulse application, and (3) suspending of cells in the pellet followed by centrifugation

Procedures	$\Delta\varepsilon_H$	f_{cH}/MHz	β_H	$\Delta\varepsilon_L$	f_{cL}/Hz	β_L	A	m
1	7970	1.46	0.91				1.5×10^{10}	1.7
2	4540	2.26	0.99	1.8×10^6	410	0.81	6.8×10^9	1.7
3	9290	1.32	0.90				1.5×10^{10}	1.7

The best-fit curves for procedures 1 and 2 are shown in Fig. 4, but not for procedure 3

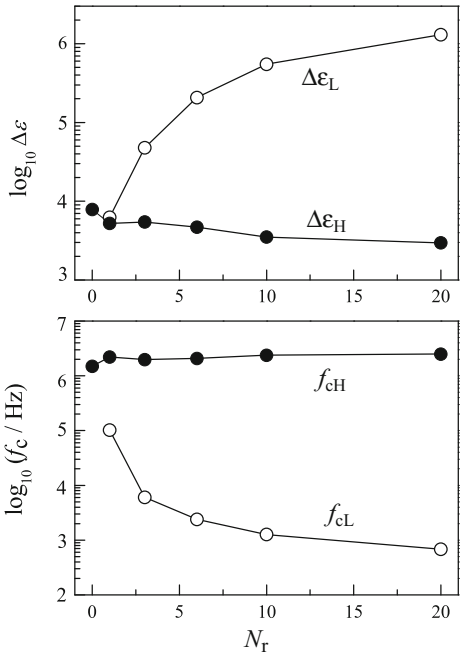

Fig. 5 Effects of the repeat counts (N_r) of AC pulses on the intensity ($\Delta\varepsilon$) and characteristic frequency (f_c) of the HF and LF relaxation

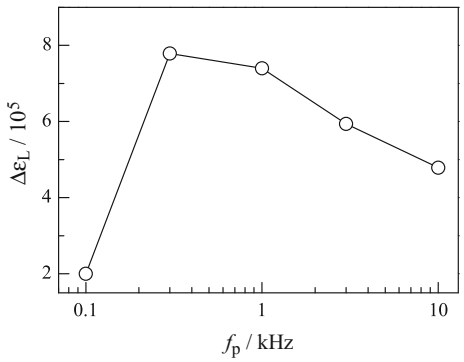

Fig. 6 Effects of frequency (f_p) of the sine wave in AC pulses on the intensity ($\Delta\varepsilon_L$) of the LF relaxation. The repeat count of AC pulses is 10

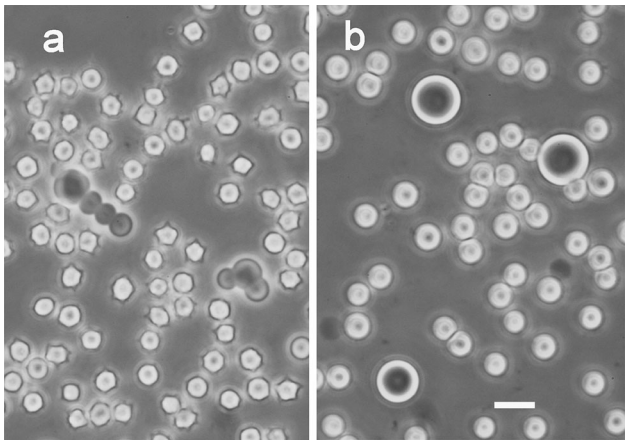

Fig. 7 Phase contrast micrographs of **a** intact and **b** heat-treated erythrocytes that were collected from the pellets after pulse application. The *scale bar* is 10 μm

multiple cells fusing together to be elongated cells that run parallel to the electric field (Chemomordik and Sowers 1991). It is probable that similar fusion products occur in the pellets.

In a previous paper (Asami 2007), numerical simulation was carried out with a cubic array of spherical cells as a model of tissues. If there is no special junction between cells, the model showed the dielectric relaxation expected for cell suspensions. When cells forming lines parallel to the electric field were connected with conducting junctions like gap junctions, dielectric relaxation appeared at lower frequencies. Numerical simulation also showed that the dielectric properties of two spherical cells that are connected through a narrow cytoplasmic junction are approximately represented by the prolate spheroidal cell model (Asami et al. 1998; Sekine et al. 2005). Watanabe et al. (1991) applied an oriented ellipsoidal cell model to the dielectric behavior of frog lens, and demonstrated that the LF relaxation is due to the polarization of fiber cells that run parallel to the applied electric field. The studies imply

that the origin of the LF relaxation found in this study is due to long fused cells that run parallel to the applied electric field, and, as a first approximation, the fused cells may be modeled by prolate spheroidal cells in the parallel orientation where the long axes are parallel to the applied electric field.

Here, an attempt was made to simulate the dielectric behavior resulting from cell electrofusion in cell pellets using an oriented ellipsoidal cell model similar to that used by Watanabe et al. (1991). Centrifugation of a cell suspension forms a pellet (thickness d_p) and a supernatant between electrodes (electrode distance d and surface area S). The admittance Y of the whole system may be represented by a serial combination of the supernatant admittance Y_{sup} and the pellet admittance Y_{pel} (Fig. 8b):

$$\frac{1}{Y} = \frac{1}{Y_{sup}} + \frac{1}{Y_{pel}}. \tag{3}$$

When the supernatant is the same as the suspending medium of complex permittivity ε_a^*, and the pellet, which is regarded as a dense cell suspension, has complex permittivity ε_{pel}^*, Y_{sup} and Y_{pel} are represented by

$$Y_{sup} = \mathrm{j}2\pi f\varepsilon_0 \frac{S}{d - d_P}\varepsilon_a^*, \tag{4}$$

$$Y_{pel} = \mathrm{j}2\pi f\varepsilon_0 \frac{S}{d_p}\varepsilon_{pel}^*. \tag{5}$$

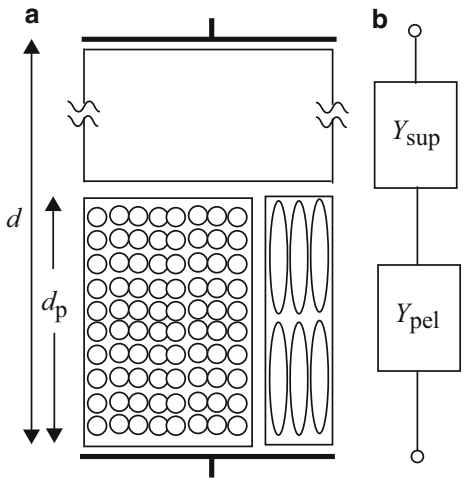

Fig. 8 Electrical model for cell electrofusion in centrifuged cell pellet. **a** A pulsed pellet of thickness d_p is modeled by a mixture of spherical cells (unfused cells) and oriented spheroidal cells (fused cells). **b** The whole system including the supernatant and the pellet is represented by a serial combination of the corresponding admittances Y_{sup} and Y_{pel}

Complex permittivity is defined as $\varepsilon^* = \varepsilon + \kappa/(\mathrm{j}2\pi f\varepsilon_0)$, where ε is relative permittivity and κ is conductivity. When the pellet contains spherical cells that correspond to unfused cells at volume fraction P, ε_{pel}^* is given by the complex permittivity ε_S^* derived for the concentrated suspension of spherical cells (Hanai et al. 1979; Asami 2002) as

$$1 - P = \left(\frac{\varepsilon_S^* - \varepsilon_{sp}^*}{\varepsilon_a^* - \varepsilon_{sp}^*}\right)\left(\frac{\varepsilon_a^*}{\varepsilon_S^*}\right)^{1/3} \tag{6}$$

with

$$\varepsilon_{sp}^* = \varepsilon_m^* \frac{2\varepsilon_m^* + \varepsilon_i^* - 2v_s(\varepsilon_m^* - \varepsilon_i^*)}{2\varepsilon_m^* + \varepsilon_i^* + v_s(\varepsilon_m^* - \varepsilon_i^*)}, \tag{7}$$

where ε_i^* and ε_m^* are the complex permittivities of the cytoplasm and the membrane, respectively, and $v_s = (1 - d_m/R)^3$ with cell radius R and membrane thickness d_m.

After pulse application, some spherical cells are fused to be prolate spheroidal cells whose symmetry axes are parallel to the applied electric field (Fig. 8a). For sake of simplicity, it is assumed that there is no change in the total cell volume in the pellet during the cell fusion; the volume fraction P of the total cells (including both the spherical and spheroidal cells) is unchanged. If the contribution of the spheroidal cells to ε_{pel}^* is proportional to the volume ratio p_E of the total spheroidal cells to the whole cells in the pellet, ε_{pel}^* is given by

$$\varepsilon_{pel}^* = p_E\varepsilon_E^* + (1 - p_E)\varepsilon_S^*, \tag{8}$$

where ε_E^* is the complex permittivity of the concentrated suspension of oriented spheroidal cells. Both ε_E^* and ε_S^* are calculated at the same volume fraction P and $\varepsilon_{pel}^* = \varepsilon_S^*$ at $p_E = 0$. ε_E^* is given by (Boyle 1985; Asami 2002)

$$1 - P = \left(\frac{\varepsilon_E^* - \varepsilon_{ep}^*}{\varepsilon_a^* - \varepsilon_{ep}^*}\right)\left(\frac{\varepsilon_a^*}{\varepsilon_E^*}\right)^{A_z}. \tag{9}$$

The effective complex permittivity ε_{ep}^* of the spheroidal cell along the z-axis (or the symmetry axis) is obtained by assuming that d_m is much smaller than R_z and R_{xy} (Asami et al. 1980).

$$\varepsilon_{ep}^* = \varepsilon_m^* \frac{\varepsilon_m^* + (\varepsilon_i^* - \varepsilon_m^*)A_z + v_e(\varepsilon_i^* - \varepsilon_m^*)(1 - A_z)}{\varepsilon_m^* + (\varepsilon_i^* - \varepsilon_m^*)A_z - v_e(\varepsilon_i^* - \varepsilon_m^*)A_z}, \tag{10}$$

where $v_e = (1 - d_m/R_z)(1 - d_m/R_{xy})^2$ with semi-axis R_z along the z-axis and semi-axis R_{xy} along the equatorial axis

(the x- and y-axes). The depolarization factor A_z along the z-axis is given as a function of $q = R_z/R_{xy}$ as

$$A_z = \frac{-1}{q^2-1} + \frac{q}{(q^2-1)^{3/2}} \ln\left[q + \left(q^2-1\right)^{1/2}\right]. \quad (11)$$

Since Y given by Eq. (3) is related to the effective complex permittivity ε^* of the whole system as $Y = j2\pi f\varepsilon_0(S/d)\varepsilon^*$, ε^* becomes

$$\varepsilon^* = \frac{\varepsilon_a^*\left[(1-p_E)\varepsilon_S^* + p_E\varepsilon_E^*\right]}{\left(1-d_p/d\right)\left[(1-p_E)\varepsilon_S^* + p_E\varepsilon_E^*\right] + \left(d_p/d\right)\varepsilon_a^*}. \quad (12)$$

In order to calculate ε^* there is a difficulty in solving Eq. (9). Numerical integration has been performed using the differential form of Eq. (9):

$$\Delta\varepsilon^* = \frac{\Delta P'}{1-P'}\left(\frac{1}{\varepsilon_{ep}^* - \varepsilon^*} + \frac{A_z}{\varepsilon^*}\right). \quad (13)$$

$\Delta\varepsilon^*$ is the increment due to a small increment of $\Delta P'$ ($\Delta P' = P/100$ for instance) in the volume fraction. Numerical integration of Eq. (13) with respect to ε^* and P' over the ranges of [ε_a^* to ε^*] and [0 to P] provides the final complex permittivity ε^* of the cell suspension at P.

Figure 9 shows the results calculated from parameter values relevant to erythrocytes as: $\varepsilon_a = 80$, $\kappa_a = 1$ S m^{-1}, $\varepsilon_i = 60$, $\kappa_i = 0.5$ S m^{-1}, $\varepsilon_m = 5$, $\kappa_m = 0$ S m^{-1} (subscripts a, i and m refer to the medium, the cytoplasm and the membrane, respectively), $d_m = 5$ nm, $P = 0.7$, $R = 3$ μm, $R_{xy} = 3$ μm, and $d_p/d = 0.2$. When the content of spheroidal cells of $R_z = 90$ μm in parallel orientation is raised by changing p_E from 0 to 0.3, the LF relaxation develops (Fig. 9a). With increasing p_E, the intensity $\Delta\varepsilon_L$ of the LF relaxation increases accompanying a decrease in the intensity $\Delta\varepsilon_H$ of the HF relaxation, whereas the characteristic frequency f_{cL} of the LF relaxation is independent of p_E. In contrast, by varying the value of R_z at a constant p_E ($p_E = 0.2$), both of the $\Delta\varepsilon_L$ and the f_{cL} are markedly changed (Fig. 9b). With increasing R_z, the $\Delta\varepsilon_L$ increases accompanying a decrease of f_{cL}, whereas the $\Delta\varepsilon_H$ is mostly unchanged. The results suggest that the $\Delta\varepsilon_L$ depends on both of p_E and R_z and that the f_{cL} is a function of R_z. The $\Delta\varepsilon_L$ and f_{cL} may be available for indexes of the content and morphology of fusion products in the pellet. Following the numerical simulation, the differences of the LF relaxation between intact and heat-treated cells shown in Figs. 2 and 3 are interpreted as follows. Since the heat treatment increased $\Delta\varepsilon_L$ and decreased f_{cL}, an increased number of heat-treated cells are fused to be longer rod-like cells. This implies that the cell fusion is facilitated by the heat treatment or is inhibited by the spectrin network.

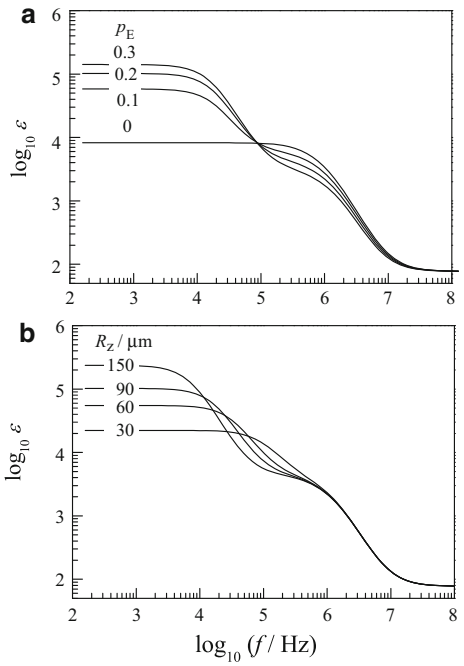

Fig. 9 Simulation of dielectric spectra for a system consisting of a centrifuged pellet and a supernatant. The pellet is a mixture of spherical cells and oriented spheroidal ones as in Fig. 8. **a** The volume ratio (p_E) of the ellipsoidal cells to the whole cell volume is varied from 0 to 0.3 as indicated. The semi-axis (R_z) along the symmetry axis is 90 μm. **b** The value of R_z is changed from 30 to 150 μm as indicated and $p_E = 0.2$

The present model, however, is not sufficient for quantitative descriptions of the morphology of the fusion products as follows: The spheroidal cell model does not provide the detailed morphology of the fusion products, e.g., fused cells are connected narrow channels, and the chains of fused cells are not necessarily linear and are widely distributed in length. Furthermore, at the present, it is difficult to deal with the electric interactions between cells in densely packed cell pellets. Therefore, it should be noted that the simulation of the dielectric spectra is liable to include considerable errors.

Next we will consider why the LF relaxation was extremely reduced in intensity when cells in the pulsed pellet were re-suspended and were centrifuged again. As shown in Fig. 7, the cells taken out of the pulsed pellets include chains of fused cells for intact cells and giant spherical cells for heat-treated cells. The centrifuged pellets of the re-suspended cells, therefore, may contain long fused cells in a different orientation from that in the previous pulsed pellet for the intact cells or giant spherical cells for the heat-treated cells. It is reasonable to suppose that the drastic changes of the LF relaxation is associated with the orientation change of the long fused cells and the cell shape change to giant spherical cells.

Using the prolate spheroidal cell model, we first examine the effects of the cell orientation. Although complicated calculations similar to those shown in Fig. 9 are possible, a simple examination has been attempted using approximate

equations that provide the dielectric relaxation parameters for dilute suspensions of spheroidal cells (Asami and Yonezawa 1995). The approximate equations are not strictly applicable to the closely packed cell pellet but are still available for qualitative examination. When prolate spheroidal cells of less conducting cell membranes are in the parallel orientation, the intensity $\Delta\varepsilon_z$ and the characteristic frequency f_{cz} are given by

$$\Delta\varepsilon_z = \frac{P\bar{R}C_m}{3\varepsilon_0}\frac{1}{A_z(1-A_z)^2}, \tag{14}$$

$$f_{cz} = \frac{3}{2\pi\bar{R}C_m}\left(\frac{1}{A_z\kappa_i}+\frac{1}{(1-A_z)\kappa_a}\right)^{-1}, \tag{15}$$

where $\bar{R} = 3\left(2/R_{xy} + 1/R_z\right)^{-1}$ and $C_m = \varepsilon_m\varepsilon_0/d_m$. In the perpendicular orientation where the z-axis is perpendicular to the applied electric field, the intensity $\Delta\varepsilon_{xy}$ and the characteristic frequency f_{cxy} become

$$\Delta\varepsilon_{xy} = \frac{P\bar{R}C_m}{3\varepsilon_0}\frac{8}{(1-A_z)(1+A_z)^2}, \tag{16}$$

$$f_{cxy} = \frac{3}{2\pi\bar{R}C_m}\left(\frac{2}{(1-A_z)\kappa_i}+\frac{2}{(1+A_z)\kappa_a}\right)^{-1}. \tag{17}$$

The values of A_z calculated from Eq. (11) is much smaller than unity for prolate spheroidal cells of a large axial ratio q ($q = R_z/R_{xy}$), e.g., $A_z = 0.003$ for $q = 30$. Thus, Eqs. (15) and (17) with $\kappa_i/\kappa_a = 1$ provide $f_{cxy}/f_{cz} \approx 1/(4A_z) \gg 1$, which indicates that dielectric relaxations for the perpendicular and parallel orientations correspond to the HF and LF relaxations, respectively. The intensity ratio between the parallel and perpendicular orientation becomes $\Delta\varepsilon_{xy}/\Delta\varepsilon_z \approx 8A_z$ using Eqs. (14) and (16); $\Delta\varepsilon_{xy}$ is much smaller than $\Delta\varepsilon_z$. In the case of the random orientation of the spheroidal cells, the intensity of the LF relaxation becomes one-third of $\Delta\varepsilon_z$ (Asami and Yonezawa 1995). It is clear that the LF relaxation is reduced in intensity by changing the cell orientation from the parallel orientation. This provides a possible account of the reduction of the LF relaxation in the centrifuged pellet formed from re-suspended cells.

The effects of the morphological change from the spheroidal cells in the parallel orientation to the giant spherical are considered for heat-treated cells. The intensity $\Delta\varepsilon_s$ and the characteristic frequency f_{cs} of dielectric relaxation for the suspension of spherical cells of radius R are obtained by putting $A_z = 1/3$ in Eqs. (14) and (15):

$$\Delta\varepsilon_s = \frac{9PRC_m}{4\varepsilon_0}, \tag{18}$$

$$f_{cs} = \frac{1}{2\pi RC_m}\left(\frac{1}{\kappa_i}+\frac{1}{2\kappa_a}\right)^{-1}. \tag{19}$$

Equations (18) and (19), which were originally derived by Pauly and Schwan (Pauly and Schwan 1959), show that $\Delta\varepsilon_s$ and f_{cs} are directly and inversely proportional to R, respectively. Since the radius of the giant spherical cells is at most five times larger than unfused cells (that provide the HF relaxation), the dielectric relaxation of the giant spherical cells appears in a frequency range not far apart from the HF relaxation. Thus, the morphological change from the spheroidal cells in the parallel orientation to the giant spherical cells may diminish the LF relaxation and increases the intensity of the HF relaxation. Equations (14) and (18) provide $\Delta\varepsilon_s/\Delta\varepsilon_z \approx (27/4)A_zR/\bar{R}$ with $\bar{R} \approx (3/2)R_{xy}$ for a large axial ratio, say $q = 30$. If the cell volume is unchanged through the morphological change, $R = (R_{xy}^2R_z)^{1/3} = R_{xy}q^{1/3}$ and $\Delta\varepsilon_s/\Delta\varepsilon_z \approx (9/2)A_zq^{1/3}$, which indicates a large reduction in relaxation intensity as a whole. The cell shape change, therefore, is a possible interpretation of the disappearance of the LF relaxation together with a small increase in the intensity of the HF relaxation (procedure 3 in Table 1). This supports the idea that long fused cells running parallel to the applied field remain in the pulsed pellet and change to giant spherical cells by releasing the fused cells from the pellet. In the pellets containing closely packed cells, limited available space between cells may prevent long rod-like fused cells from being giant spheres.

Concluding Remarks

This study has demonstrated that dielectric spectroscopy is a useful technique for in situ and non-invasive monitoring of fusion products in centrifuged cell pellets. The LF relaxation induced by pulse application was due to the fusion products and was seriously affected by heat treatment of cells and the conditions of the applied pulses. The theoretical simulation using the oriented spheroidal cell model for fused cells showed that the LF relaxation is sensitive to the morphology and the content of fusion products. The relaxation parameters of the LF relaxation, therefore, are useful for characterizing the fusion products.

Although the measurement technique used in this study was not applied to early events within 10 s after pulse

application, technical improvements should enable us to study the initial fusion processes including the occurrence of pores on the contact zone between cells and the expansion of the pores to yield giant cells.

References

Abidor IG, Barbul AI, Zhelev DV, Doinov P, Bandrina IN, Osipova EM, Sukharev SI (1993) Electrical properties of cell pellets and cell electrofusion in a centrifuge. Biochim Biophys Acta 1152:207–218

Abidor IG, Li LH, Hui SW (1994) Studies of cell pellets: II. Osmotic properties, electroporation and related phenomena: membrane interactions. Biophys J 67:427–435

Asami K (2002) Characterization of heterogeneous systems by dielectric spectroscopy. Prog Polym Sci 27:1617–1659

Asami K (2007) Dielectric properties of biological tissues in which cells are connected by communicating junctions. J Phys D 40:3718–3727

Asami K (2012) Dielectric spectroscopy reveals nanoholes in erythrocyte ghosts. Soft Matter 8:3250–3257

Asami K, Sekine K (2007a) Dielectric modeling of cell division for budding and fission yeast. J Phys D 40:1128–1133

Asami K, Sekine K (2007b) Dielectric modeling of erythrocyte aggregation in blood. J Phys D 40:2197–2204

Asami K, Yonezawa T (1995) Dielectric behavior of non-spherical cells in culture. Biochim Biophys Acta 1245:317–324

Asami K, Hanai T, Koizumi N (1980) Dielectric approach to suspensions of ellipsoidal particles covered with a shell in particular reference to biological cells. Jpn J Appl Phys 19:359–365

Asami K, Gheorghiu E, Yonezawa T (1998) Dielectric behavior of budding yeast in cell separation. Biochim Biophys Acta 1381:234–240

Asami K, Gheorghiu E, Yonezawa T (1999) Real-time monitoring of yeast cell division by dielectric spectroscopy. Biophys J 76:3345–3348

Boyle MH (1985) The electrical properties of heterogeneous mixture containing an oriented spheroidal dispersed phase. Colloid Polym Sci 263:51–57

Chemomordik LV, Sowers AE (1991) Evidence that the spectrin network and a nonosmotic force control the fusion product morphology in electrofused erythrocyte ghosts. Biophys J 60:1026–1037

Daoud J, Asami K, Rosenberg L, Tabrizian M (2012) Dielectric spectroscopy for non-invasive monitoring of epithelial cell differentiation within three-dimensional scaffolds. Phys Med Biol 57:5097–5112

Finaz C, Lefevre A, Teissie J (1984) Electrofusion. A new, highly efficient technique for generating somatic cell hybrids. Exp Cell Res 150:477–482

Glaser RW, Donath E (1987) Hindrance of red cell electrofusion by the cytoskeleton. Stud Biophys 121:37–43

Hanai T, Asami K, Koizumi N (1979) Dielectric theory of concentrated suspension of shell-spheres in particular reference to the analysis of biological cell suspensions. Bull Inst Chem Res Kyoto Univ 57:297–305

Hayashi Y, Katsumoto Y, Omori S, Yasuda A, Asami K, Kaibara M, Uchimura I (2010) Dielectric coagulometry: a new approach to estimate venous thrombosis risk. Anal Chem 80:9769–9774

Irimajiri A, Ando M, Matsuoka R, Ichinowatari T, Takeuchi S (1996) Dielectric monitoring of rouleaux formation in human whole blood: a feasibility study. Biochim Biophys Acta 1290:207–209

Jaroszeski MJ, Gilbert R, Fallon PG, Helier R (1994) Mechanically facilitated cell-cell electrofusion. Biophys J 67:1574–1581

Jaroszynski W, Keslinka E, Wujtewicz M, Suchorzewska J, Kwiatkowski B (2002) Effects of hydroxyethyl starch (HAES) on degree and kinetics of erythrocyte aggregation studied with dielectric spectroscopy method. Med Sci Monit 8:272–278

Li LH, Hensen ML, Zhao YL, Hui SW (1996) Electrofusion between heterogeneous-sized mammalian cells in a pellet: potential application in drug delivery and hybridoma formation. Biophys J 71:479–486

Mekid H, Mir LM (2000) In vivo cell electrofusion. Biochim Biophys Acta 1524:118–130

Pauly H, Schwan HP (1959) Über die Impedanz einer Suspension von kugelformigen Teilchen mit einer Schale. Z Naturforsch B 14:125–131

Salomskaite-Davalgiene S, Cepurniene K, Satkkauskas S, Venslauskas MS, Mir LM (2009) Extent of cell electrofusion in vitro and in vivo is cell line dependent. Anticancer Res 29:3125–3130

Sekine K, Watanabe Y, Hara S, Asami K (2005) Boundary-element calculations for dielectric behavior of doublet-shaped cells. Biochim Biophys Acta 1721:130–138

Takahashi Y, Suzuki K, Niimura T, Kano T, Takashima S (1991) A production of monoclonal antibodies by a simple electrofusion technique induced by ac pulses. Biotechnol Bioeng 37:790–794

Terpitz U, Letschert S, Bonda U, Spahn C, Guan C, Sauer M, Zimmermann U, Bamberg E, Zimmermann D, Sukhorukov VL (2012) Dielectric analysis and multi-cell electrofusion of the yeast *Pichia pastoris* for electrophysiological studies. J Membr Biol 245:815–826

Usaj M, Trontelj K, Miklavcic D, Kanduser M (2010) Cell-cell electrofusion: optimization of electric field amplitude and hypotonic treatment for mouse melanoma (B16-F1) and Chinese Hamster Ovary (CHO) cells. J Membr Biol 236:107–116

Watanabe M, Suzaki T, Irimajiri A (1991) Dielectric behavior of the frog lens in the 100 Hz to 500 MHz range. Simulation with an allocated ellipsoidal-shells model. Biophys J 59:139–149

Zimmermann U (1982) Electric field-induced cell-to-cell fusion. J Membr Biol 64:165–182